Homoclinic tangency and chaotic attractor disappearance in a dripping faucet experiment

Reynaldo D. Pinto* and José C. Sartorelli†
Instituto de Física, Universidade de São Paulo, Caixa Postal 66318, 05315-970 São Paulo, SP, Brazil
(Received 20 July 1999)

A sequence of attractors, reconstructed from interdrops time series data of a leaky faucet experiment, is analyzed as a function of the mean dripping rate. We established the presence of a saddle point and its manifolds in the attractors and we explained the dynamical changes in the system using the evolution of the manifolds of the saddle point, as suggested by the orbits traced in first return maps. The sequence starts at a fixed point and evolves to an invariant torus of increasing diameter (a Hopf bifurcation) that pushes the unstable manifold towards the stable one. The torus breaks up and the system shows a chaotic attractor bounded by the unstable manifold of the saddle. With the attractor expansion the unstable manifold becomes tangential to the stable one, giving rise to the sudden disappearance of the chaotic attractor, which is an experimental observation of a so called chaotic blue sky catastrophe.

PACS number(s): 05.45.−a, 47.55.Dz

The theory of nonlinear dynamical systems [1,2] has merged problems of totally different subjects in a common frame: the quadratic map came from population dynamics models [3]; the Van de Pol oscillator was derived from a heart model [3]; neural networks are simplifications of ideas from neuroscience [3]; methods of control of chaos have been applied to cardiac arrhythmia [4] and epileptic diseases [5]. A sudden disappearance of a chaotic attractor, a chaotic blue sky catastrophe [6–8], which occurs due to a homoclinic tangency between the manifolds of a saddle point was found in simulations of the Van der Pol oscillator. Tangencies between manifolds of chaotic attractors play important roles in dynamical systems [9]; attractors which present homoclinic tangencies are called quasiattractors [10,11] (abbreviation, of ''quasistochastic attractors''), they are structurally unstable and their applications concern the understanding of the biological memory mechanisms [1].

Although dripping faucets do not belong to the class of systems whose dynamics is the result of evolutionary processes, as the biological systems, the time series of interdrop intervals [12] has shown the same power law long-range anticorrelations and non-Gaussian behavior presented by the time series of interbeat intervals of healthy hearts [13]. Another similarity between attractors of dripping faucets and the biological ones was found in recent studies on an isolated colony of ants, where explorative behavior was stimulated [14]. Nevertheless, there is no model or explanation for the similarities found between dripping faucet experiments and biological systems.

In 1977, it was suggested [15] that a dripping faucet could present complex behavior. The first dripping faucet experiment was reported in 1985 [16] and a simple mass-spring model was used to explain a few features of the dripping dynamics. Since then, a wide range of nonlinear behaviors has been observed, such as strange attractors [17–20], satellite drops formation [21], bifurcations [22,23], crises and intermittencies [18,20], long-range anticorrelations [22], and scale laws [23].

As a successful and comprehensive interpretation of the drop formation dynamics by analytical models or computational simulations [16,24,25] has not been achieved yet, we have applied topological analysis to sequences of attractors (first-return maps T_{n+1} vs T_n) reconstructed from series $\{T_n\}$ of the delay time between successive drops.

The measurements were made with the faucet attached to a large reservoir, see Refs. [18,19] for details. In our experiment the faucet is a cylindrical glass nozzle (3 mm inner diameter) attached to a deionized water reservoir (800 l). The delay time between successive drops was measured with a time counter circuitry, with a resolution of $1\,\mu$s, inserted in a PC slot. The input signals are voltage pulses, induced in a resistor, defined by the beginning (ending) of the scattering of a laser beam focused on a phototransistor (in series with the resistor) when the drop starts (ends) to cross the laser beam. The width of the pulse is the time interval t_n (where n is the drop number), and the delay time between two pulses is the crossing time (δt_n), of a drop through the laser beam, so that the total time interval is $T_n = t_n + \delta t_n$. We can setup the drop rate ($f = 1/\langle T \rangle$) in two ways: (a) by feeding back the water reservoir to keep the height h of the water level and selecting the drop rate by opening (closing) a needle valve driven by a step motor which is controlled by a microcomputer. For a given drop rate we have constructed first return maps T_{n+1} vs T_n; (b) by fixing the opening of the needle valve, turning off the water supply, letting the water level decrease naturally, and so the dripping rate. Therefore, the control parameter, the height h of the water level, varies as $h \approx h_0 - n\,\delta V/A$, where h_0 is the initial height, δV the drops mean volume, and A is the area of the water reservoir surface. In this case, bifurcation diagrams T_n vs n were constructed.

A little bit above 40 drops/s the water flux becomes continuous at the laser-detector level. Therefore, we opened the faucet, reaching a dripping rate just before the water flux became continuous. For an overview, we took first a time

*Electronic address: reynaldo@fge.if.usp.br
†Electronic address: sartorelli@if.usp.br

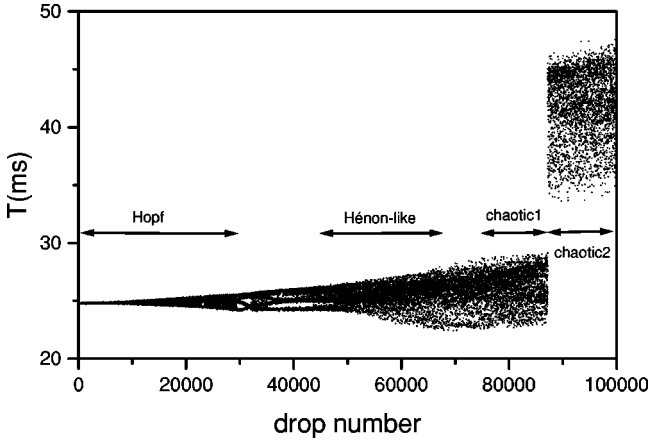

FIG. 1. Bifurcation diagram obtained by letting the water level of a 50l reservoirs decrease naturally with the dripping. The time series $\{T_n\}$ is 100 000 drops long, but we plotted just one point every four to let the figure clear.

series with the nozzle attached to a smaller reservoir (50 l) and we turned the water supply off to obtain the bifurcation diagram T_n vs. n shown in Fig. 1. Four different behaviors were identified: Hopf, Hénon-like, chaotic 1 and chaotic 2 as a function of the water level decreasing. It was observed a sudden change in the mean drop frequency, and the orbits jump from chaotic 1 to the chaotic 2 region, generating another attractors profile.

In order to investigate the route following the successive attractors, we repeated the measurements with the nozzle attached to a large water reservoir (800 l) and turning the water supply on. As before, we setup the system to the highest dripping rate, and we closed the faucet step by step. Immediately after each step, we took a series 65 536 interdrop times long. As we had already known that the system requires a long time to stabilize, we subdivided each series in an unstable subseries taking the first 16 384 points, and in a stable sub-series taking the last 16 384 interdrop times. A sequence of 49 stable series, named B0 (39.46 drops/s) up to B48 (24.78 drops/s), was obtained. In this way, we obtained the behaviors sequence: a stable fixed point, Hopf bifurcation, Hénon-like, chaotic 1, and chaotic 2, as before. The mean drop rate decreases smoothly until the end of the chaotic 1 region when a sudden change in the dripping rate occurs, from 37.29 drops/s to 24.93 drops/s. After the transition we went back by opening the faucet, and we found a hysteresis of 40 steps to achieve both the transition to higher dripping rates and the attractors profile at the end of the chaotic 1 region.

Figure 2(a) shows the reconstruction [26] (first return map T_{n+1} vs T_n) of the dynamical attractor corresponding to the unstable subseries B44, in which the control parameter varies so slowly that one can follow the sudden change in the attractors behavior. By tracing some orbits, as shown in small black arrows in Fig. 2(b), we obtained evidences for the existence of a saddle point S1 at (29 ms, 29 ms) position, represented by an open star. The gray large arrows are local representations of the unstable manifolds of S1 while the black ones are local representations of the stable manifolds. To confirm the existence of this saddle point we looked for a numerical method to extract unstable periodic orbits embedded in a chaotic attractor.

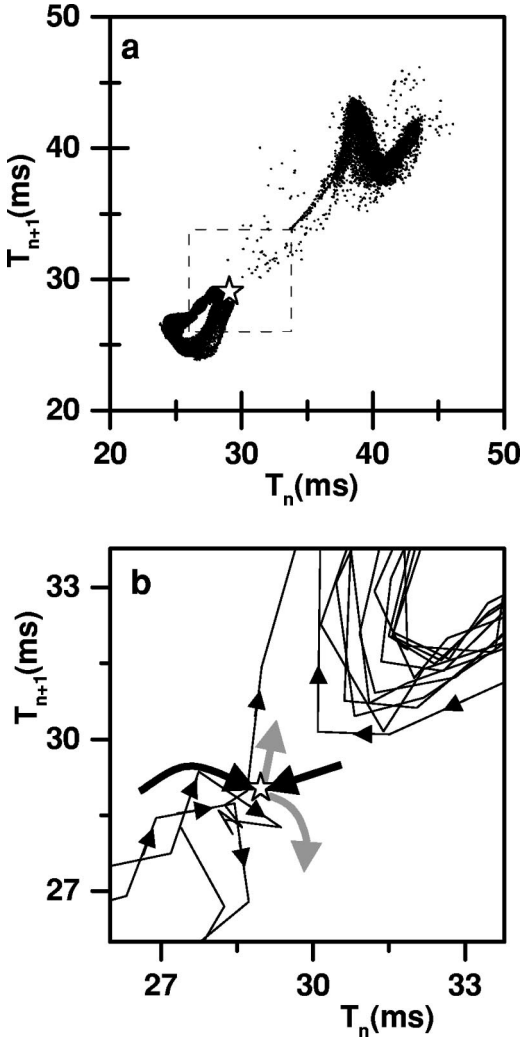

FIG. 2. (a) First return map of the transient subseries B44. (b) Enlarged view of the square region above. The saddle point S1 at ($\sim$29 ms, $\sim$29 ms) is represented by a star. The gray (black) lines are pictorial representations of the local unstable (stable) manifolds. The saddle point and its manifolds were inferred following the orbits represented by the smaller black arrows.

So *et al.* [27–29] supposed that all points lying in a region around the fixed point $x^*=f(x^*)$ can be transformed to $\{\hat{x}_n\}$ in the vicinity of x^* to extract the unstable periodic orbits (UPO's) from a finite amount of data of a one-dimensional system. The density function $\hat{\rho}(\hat{x})$ has inverse square root type singularities at the fixed points, and a histogram plot approximation to $\hat{\rho}(\hat{x})$ will have a sharp peak at $\hat{x}=x^*$. Some spurious peaks appear in $\hat{\rho}(\hat{x})$ either due to singularities not related to fixed points, or due to zeros of the derivative of the transformation function $\hat{x}=g(x,k)$. They generalized the method for a system with an arbitrary embedded dimension (d) to obtain the unstable periodic orbits by doing the transformation

$$\hat{\mathbf{z}}_n=(\mathbf{1}-\mathbf{S}_n)^{-1}(\mathbf{z}_{n+1}-\mathbf{S}_n\mathbf{z}_n), \tag{1}$$

where

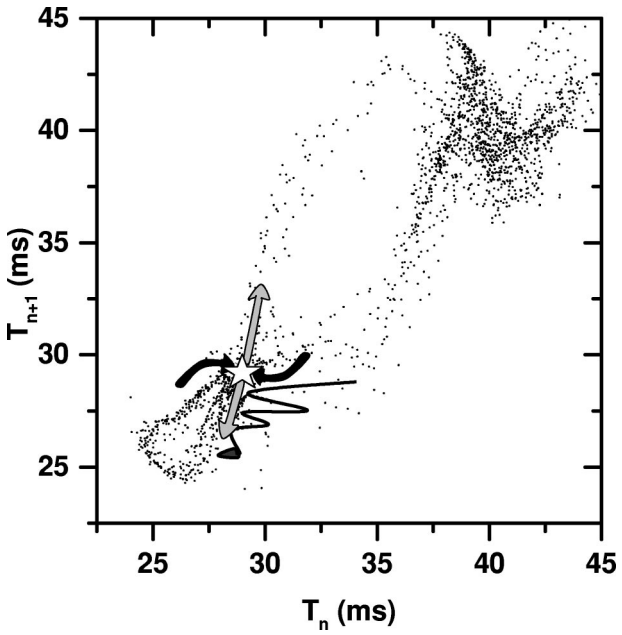

FIG. 3. First return map of the time series obtained at the transition region with the faucet nozzle inclined four degrees with the vertical. The black and gray arrows represent the local directions followed by many orbits, which allowed us to infer the saddle point position, represented by a star, while the thin black line represents the directions followed in the transition chaotic 2→chaotic 1. The time series $\{T_n\}$ is 16 384 drops long, but we plotted just the first 2048 points to let the figure clear.

$$\mathbf{S}_n=\begin{pmatrix} a_n^1 a_n^2 \cdots a_n^{(d-1)} & a_n^d \\ \mathbf{1} & \mathbf{0} \end{pmatrix}+\kappa\mathbf{R}||\mathbf{z}_{n+1}-\mathbf{z}_n||, \qquad (2)$$

$$\begin{pmatrix} a_n^1 \\ \cdot \\ \cdot \\ \cdot \\ a_n^d \end{pmatrix}=\begin{pmatrix} (\mathbf{z}_n-\mathbf{z}_{n-1})^\dagger \\ \cdot \\ \cdot \\ \cdot \\ (\mathbf{z}_{n-(d-1)}-\mathbf{z}_{n-d})^\dagger \end{pmatrix}^{-1} \times\begin{pmatrix} (z_{n+1}^1-z_n^1)^\dagger \\ \cdot \\ \cdot \\ \cdot \\ (z_{n-(d-2)}^1-z_{n-(d-1)}^1)^\dagger \end{pmatrix}, \qquad (3)$$

$\{\mathbf{z}_n\}$ are the reconstructed vectors from scalar time series $\{x_n\}$,

$$\mathbf{z}_n=(z_n^1,z_n^2,z_n^2,\ldots,z_n^d)^\dagger=(x_n,x_{n-1},x_{n-2},\ldots,x_{n-d-1})^\dagger, \qquad (4)$$

$\mathbf{R}$ is a $d\times d$ random matrix in the range $[-1,1]$ and κ is the magnitude of the randomization. The fixed points are given by the peak positions of $\hat{\rho}(\hat{\mathbf{z}})$. As the locations of the spurious peaks depend on the k parameter, they are eliminated by taking the average $\langle\hat{\rho}(\hat{\mathbf{z}})\rangle$ for many different values picked up randomly. As the attractors reconstruction in two-dimensional embedded space are enough unfolded, we applied this technique for the parameter values: $d=2$. We also used $\kappa=5$, and 100 random matrices.

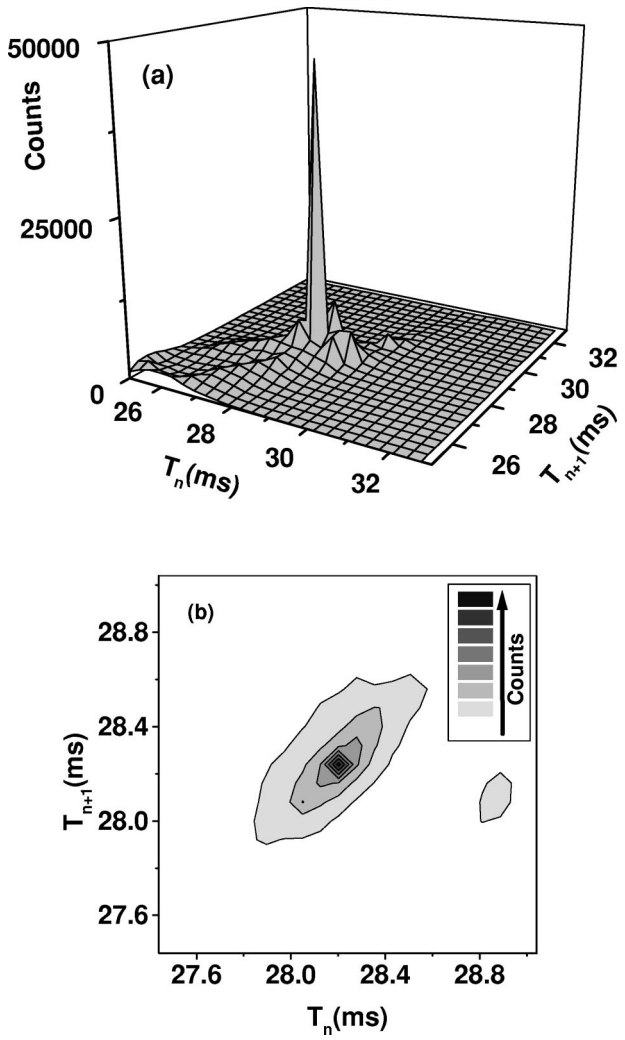

FIG. 4. (a) Histogram obtained applying the fixed point transformation to the data shown in Fig. 3. The S1 saddle point is given by the sharp peak position. (b) Corresponding contour graph to localize the peak position at (~28.3 ms, ~28.3 ms).

Therefore, the method above requires that the neighborhood of the UPO be visited many times, but in our case the orbit pass just once close to the saddle point when the B43-B44 transition occurs. We could not apply any kind of perturbations to push the orbits to the neighborhood of S1 because any small perturbation on the hanged water column is enough to precipitate the B43-B44 transition. Nevertheless, we could push the orbits to the neighborhood of the saddle point by inclining the faucet nozzle four degrees with the vertical. In this condition, both attractors are now visited in an intermittent way, as shown in Fig. 3 instead of the sudden transition shown in Fig. 2(a). The orbits return from chaotic 2 region to the chaotic 1 region through the strong folds (thin black line in Fig. 3) at the right of the chaotic 1 region. To establish the saddle point position embedded in the first return map of the series shown in Fig. 3, we applied the fixed point transform technique developed by So *et al.* [27–29], and in Fig. 4(a) is shown the histogram approximation to $\hat{\rho}(\hat{\mathbf{z}})$, the strong sharp peak corresponds to the saddle point. For better visualization of the peak position is shown in Fig.

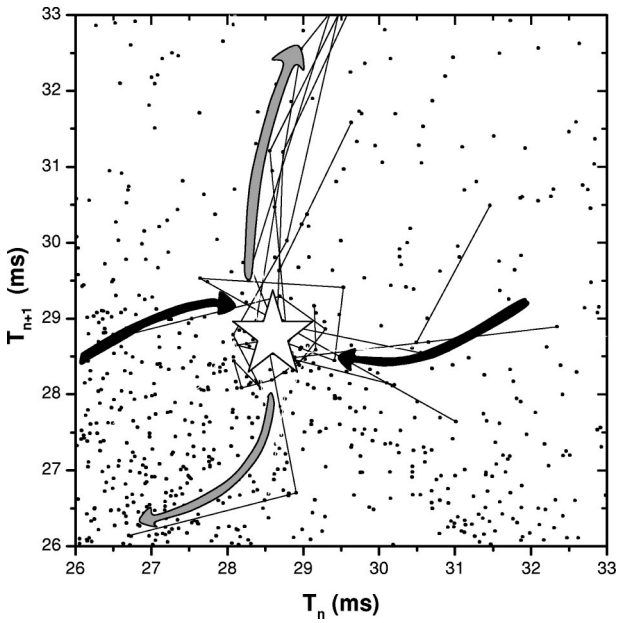

FIG. 5. First return map of the B0p series obtained by tapping the nozzle with the finger tip to destabilize the B0 stable fixed point. The black and gray arrows represent the local directions followed by many orbits (thin black lines), which allowed us to infer the saddle point position, represented by a star.

4(b) the contour graphs around the saddle point at (28.3 ms, 28.3 ms) position. In Fig. 3 we have also drawn the manifolds of the saddle point, compatible with the trace of some orbits. The strong folds of the returning orbits, represented by a black line, is an evidence of the occurrence of a homoclinic tangency of the S1 manifolds.

We also verified if this saddle point remains in other higher dripping attractors. We setup the system to reproduce the B0 stable fixed point , and then we disturbed the hanged water column by tapping the nozzle with the finger tip. The orbit spread and after then returned to the stable fixed point. The returning orbits were traced, as shown in Fig. 5. We applied again the fixed point transform technique to find the saddle point position of the B0p series. In Fig. 6(a) is shown the histogram with a strong sharp peak at (28.8 ms, 28.8 ms). As before, for better visualization of the peak position, in Fig. 6(b) is shown the contour graphs around the saddle point at (28.8 ms, 28.8 ms) position.

Therefore, we perturbed two different attractors in two different ways and we localized two saddle point positions with a little difference between them, probably due to the different systems parameters setup. Consequently, the results above leaded us to postulate that the saddle point S1 exists, at least from the stable fixed point up to the end of the chaotic 1 region, to explain the dynamics by the evolution of the S1 manifolds, which are represented by the green lines (stable manifold) and the blue lines (unstable manifold) in Fig. 7.

The first region of the sequence (B0–B48) starts with a stable focus, as shown in Fig. 7(a). The stable focus attracts the orbits from the spiraling unstable manifold of the saddle S1. As the dripping rate goes down, by closing the faucet, the focus looses its stability [22,23] becoming an unstable focus and the attractor turns into an invariant torus of increasing diameter, which characterizes a secondary Hopf bi-

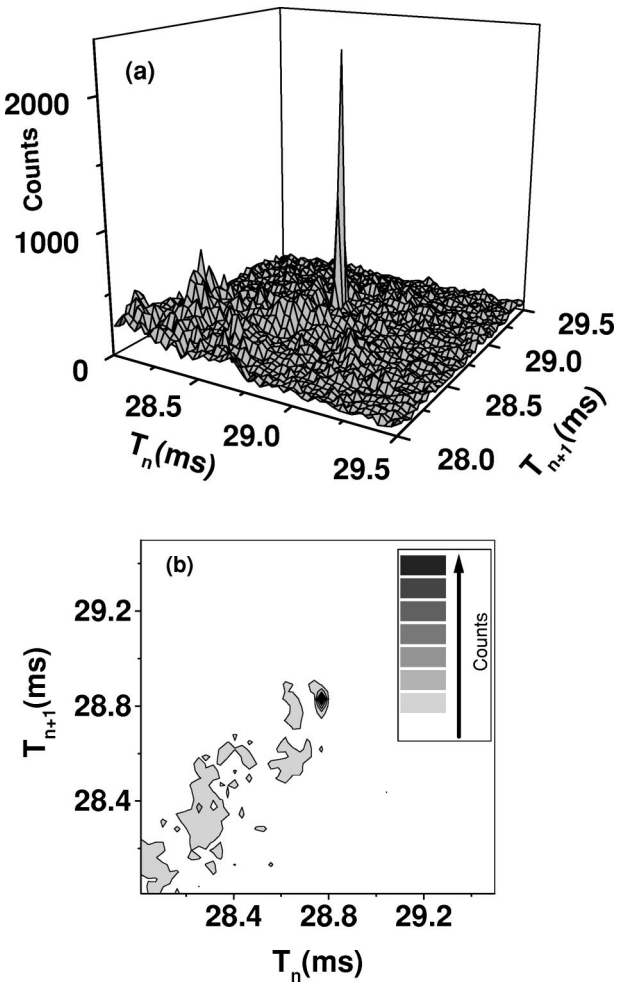

FIG. 6. (a) Histogram obtained applying the fixed point transformation to the data shown in Fig. 5. The S1 saddle point is given by the sharp peak position. (b) Corresponding contour graph to localize the peak position at (~28.8 ms, ~28.8 ms).

furcation. A torus attractor (subseries B10) from the Hopf region, as well as the unstable manifold of S1 being pushed toward the stable manifold by the torus enlargement are shown in Fig. 7(b). The torus breaks up [30,31], and the Hopf region evolves to the 5-Hénon-like region (from ~B14 up to B30), where the first return maps resemble a period-5 behavior, as exemplified in Fig. 7(c), but each branch is a Hénon-like attractor [32,33]. The increase of the size of the whole attractor continues to push the unstable manifold as before and the folds become stronger.

In Fig. 7(d) it is shown the first attractor in the chaotic 1 region while in Fig. 7(e) it is shown the last one. Since the attractors stay expanding and pushing the unstable manifold of S1 against its stable manifold the folding becomes more complex. In the last case the manifolds of S1 are about to touch each other, which characterizes a homoclinic tangency. By closing the faucet just one more step and following the unstable subseries B44 we observed that the orbits remain on the former attractor (B43) until the off-tangency takes place. The orbit crosses the stable manifold and reaches a phase space new region not accessible before, originating the chaotic 2 region of lower dripping rate. Just before the tangency, the stable manifold is a separatrix of the chaotic 1 region and the chaotic 2 one. The transition chaotic 1→chaotic 2, where

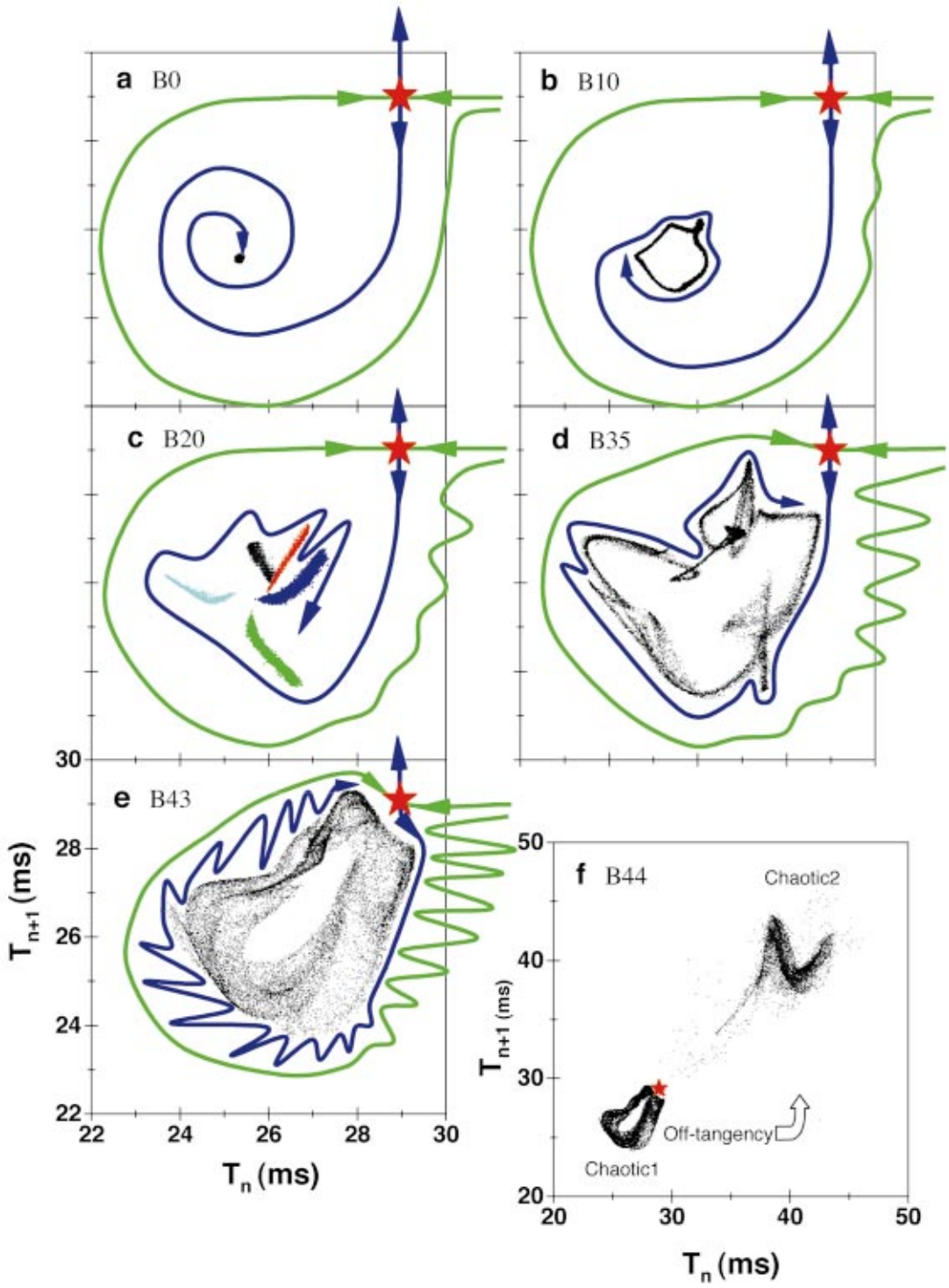

FIG. 7. (Color). Evolution to a blue sky catastrophe by following the first return maps as a function of the faucet closing. All graphs are in the same scale, except the last one. The red star represents the saddle point S1, the blue (green) lines are pictorial representations of the unstable (stable) manifolds suggested by the orbits and the dynamical evolution. (a) a stable focus. (b) a torus in the Hopf region and the beginning of the representation of the folds due to the torus enlargement that pushes the unstable manifold toward the stable one. (c) a 5-Hénon-like attractor generated by the tangency of the torus with the unstable manifold. (d) the first attractor in the chaotic 1 region and in (e), the last chaotic 1 attractor where the manifolds are close to the tangency. In (f), with the off-tangency of the manifolds the orbits migrate to the new chaotic 2 region, characterizing a chaotic blue sky catastrophe.

a chaotic attractor disappears suddenly, and the hysteresis observed are consistent with a chaotic blue sky catastrophe [6–8].

In conclusion, we could detect a saddle point by perturbing the drops formation dynamics in two different ways. In one case, the perturbation was to take off the nozzle a little from its vertical position to force the orbits to pass close to the saddle point. In the other one, we just spread out the orbits from the stable focus to observe their returning to the initial position. Postulating that the saddle point remains

from the chaotic 1 region up to stable fixed point, we applied topological analysis to the sequence of attractors to characterize a sudden disappearance of a chaotic attractor called a chaotic blue sky catastrophe, theoretically obtained from a model derived from the Van der Pol oscillator (a heart model). The occurrence of homoclinic tangencies in the dripping faucet dynamics can be one of the reasons for the relations found between dripping faucets and biological systems.

Financial support from the Brazilian Agencies FAPESP, CNPq, and FINEP is gratefully acknowledged.

[1] C. Mira, Int. J. Bifurcation Chaos Appl. Sci. Eng. **7**, 2145 (1997).
[2] K. T. Alligood, T. D. Sauer, and J. A. Yorke, *Chaos—An Introduction to Dynamical Systems* (Springer-Verlag, New York, 1997).
[3] A.V. Holden, Int. J. Bifurcation Chaos Appl. Sci. Eng. **7**, 2075 (1997).
[4] A. Garfinkel, M. L. Spano, W. L. Ditto, and J. Weiss, Science **257**, 1230 (1992).
[5] S. J. Schiff, K. Jerger, D. H. Duong, T. Chang, M. L. Spano, and W. L. Ditto, Nature (London) **370**, 615 (1994).
[6] R. A. Abraham and H. B. Stewart, Physica D **21**, 394 (1986).
[7] R. A. Abraham and C. D. Shaw, *Dynamics: The Geometry of Behavior* (Addison-Wesley, Redwood City, 1992).
[8] L. Shilnikov, Int. J. Bifurcation Chaos Appl. Sci. Eng. **7**, 1953 (1997).
[9] C. Robert, K. T. Alligood, E. Ott, and J. A. Yorke, Phys. Rev. Lett. **80**, 4867 (1998).
[10] V. S. Afraimovitch and L. P. Shilnikov, in *Nonlinear Dynamics and Turbulence* (Pitman, Boston, 1983).
[11] L. P. Shilnikov, Int. J. Bifurcation Chaos Appl. Sci. Eng. **4**, 489 (1994).
[12] T. J. P. Penna, P. M. C. de Oliveira, J. C. Sartorelli, W. M. Gonçalves, and R. D. Pinto, Phys. Rev. E **52**, R2168 (1995).
[13] C.-K. Peng, J. Mietus, J. M. Hausdorff, S. Havlin, H. E. Stanley, and A. L. Goldberger, Phys. Rev. Lett. **70**, 1343 (1993).
[14] E. Bonabeau, G. Theraulaz, J.-L. Deneubourg, A. Lioni, F. Libert, C. Sauwens, and L. Passera, Phys. Rev. E **57**, 5904 (1998).
[15] O. Rössler, in *Synergetics: A Workshop*, edited by H. Haken (Springer, Berlin, 1977).
[16] P. Martien, S. C. Pope, P. L. Scott, and R. S. Shaw, Phys. Lett. **110A**, 399 (1985).
[17] X. Wu and Z. A. Schelly, Physica D **40**, 433 (1989).
[18] J. C. Sartorelli, W. M. Gonçalves, and R. D. Pinto, Phys. Rev. E **49**, 3963 (1994).
[19] M. S. F. da Rocha, J. C. Sartorelli, W. M. Gonçalves, and R. D. Pinto, Phys. Rev. E **54**, 2378 (1996).
[20] R. D. Pinto, W. M. Gonçalves, J. C. Sartorelli, I. L. Caldas, and M. S. Baptista, Phys. Rev. E **58**, 4009 (1998).
[21] M. S. F. da Rocha, J. C. Sartorelli, W. M. Gonçalves, and R. D. Pinto, Phys. Rev. E **54**, 2378 (1996).
[22] R. D. Pinto, W. M. Gonçalves, J. C. Sartorelli, and M. J. de Oliveira, Phys. Rev. E **52**, 6896 (1995).
[23] J. G. M. da Silva, J. C. Sartorelli, W. M. Gonçalves, and R. D. Pinto, Phys. Lett. A **226**, 269 (1996).
[24] X. D. Shi, M. P. Brenner, and S. R. Nagel, Science **265**, 219 (1994).
[25] P. M. C. de Oliveira and T. J. P. Penna, Int. J. Mod. Phys. C **5**, 997 (1994).
[26] T. Sauer, in *Nonlinear Dynamics and Time Series*, edited by C. D. Cutler and D. T. Kaplan (American Mathematical Society, Providence, RI, 1997).
[27] P. So, E. Ott, S. J. Schiff, D. T. Kaplan, T. Sauer, and C. Grebogi, Phys. Rev. Lett. **376**, 4705 (1996).
[28] P. So, E. Ott, T. Sauer, B. J. Gluckman, C. Grebogi, and S. J. Schiff, Phys. Rev. E **55**, 5398 (1997).
[29] P. So, J. T. Francis, T. I. Netoff, B. J. Gluckman, and S. J. Schiff, Biophys. J. **374**, 2776 (1998).
[30] S. Ostlund, D. Rand, J. Sethna, and E. Siggia, Physica D **8**, 303 (1983).
[31] D. G. Aronson, M. A. Chory, G. R. Hall, and R. P. McGehee, Commun. Math. Phys. **83**, 303 (1982).
[32] R. Ures, Ergod. Theor. Dyn. Syst. **15**, 1223 (1995).
[33] S. V. Gonchenko and L. P. Shil'nikov, Int. J. Bifurcation Chaos Appl. Sci. Eng. **5**, 819 (1995).